An Experimental Investigation of the Dynamics of the MSL Rover Landing Event

Christopher V. White*,
Jet Propulsion Laboratory, California Institute of Technology, Pasadena, CA 91109

Keith van der Walde†, Jeffery Tippmann‡
ATA Engineering, Inc., San Diego, CA 92130

A developmental test program was conducted for the touchdown event of the Mars Science Laboratory rover. The test hardware consisted of a full-size 3/8th mass scaled test rover, a descent stage mass mock-up, and a Vectran triple-bridle system over 6 meters in length. More than eighty landing tests were performed on terrains of various types, including level rigid surfaces, level and sloped sand surfaces, and level and sloped surfaces with rocks. Landing velocities ranged between 0.4 m/s and 1.4 m/s. A computational model of the landings was developed using the ADAMS analysis program, and validation of this model has been performed through test-analysis comparisons.

I. Background and Objectives

The Mars Science Laboratory mission, scheduled for touchdown on the Martian surface in 2010, will be the first planetary spacecraft to use the Skycrane landing maneuver[1]. A central feature of Skycrane is the decoupling of the retrorocket propulsion system from the detailed motions of the vehicle during touchdown. The system architecture also merges the previously separate functionality of a rover and a lander, requiring the landing loads to pass through the mobility subsystem.

Due to the criticality of the touchdown event, and the novelty of the Skycrane, the MSL project embarked on a Touchdown Test Program during the preliminary design phase of the project. The test program had several main objectives, including the following: (1) observe and understand the performance of the rover as a landing system, (2) provide a rational basis for correlating and updating the ADAMS computer model, (3) characterize the rover system stiffness and damping, and (4) to the extent possible, validate the processes used for predicting touchdown loads and stability[2].

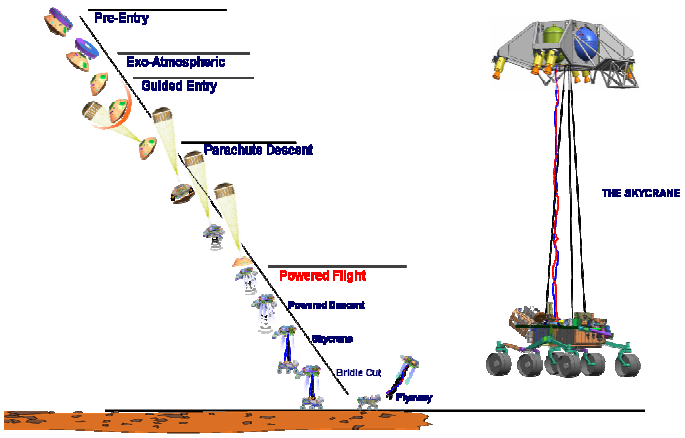


Figure 1. MSL's Entry, Descent & Landing sequence, showing the innovative Skycrane landing concept.

The hardware required to replicate a Skycrane touchdown event includes the descent stage, the triple-bridle system, and the rover. A simple mass mock-up of the descent stage stood in for the actively controlled retrorocket-propelled descent stage of the flight system. The rover was hung from Vectran bridles over 6 m in length. Central to the test program was a full-scale rover vehicle nicknamed SCARECROW. This vehicle couples an accurate build of the mobility system at the preliminary design level with a simple chassis structure which provides structural integrity and mass balance. The vehicle has near full functionality for touchdown, plus drive and steer actuators to allow testing of traverse maneuvers and mobility. The entire system is suspended above

* Senior Engineer, Mechanical Systems Division, Entry, Descent & Landing. M/S 303-410
† Project Engineer, Design and Analysis Group
‡ Engineer, Aerospace Analysis Group

the descent stage and raised and lowered by a 20 HP electric winch.

From the loads and stability perspective, the rover-as-lander architecture presents many challenges. Compared to legged landers[3], whose structural configuration remains essentially unchanged during landing, the rover presents both a flexible structure and an articulating mechanism, with large displacements and geometrically nonlinear response. Furthermore, many degrees of freedom are required to capture the response, load paths are much more complicated, and many more loads and response points are of interest. The persistence of overhead bridle loads during touchdown is another distinguishing feature. Accurate landing load predictions require accurate bridle load models. Compared to airbag landing systems[4], the Skycrane is more amenable to conventional computational methods, to such an extent that the design process can largely take place using numerically estimated loads. In this case, the role of testing is to primarily check or corroborate the numerical models and to provide data for conditions that cannot be modeled. Because the job of generating design loads falls mostly in the numerical realm, complete and accurate scaling of the Mars environment is less critical for the tests.

The test program followed a path of progressive complexity, in which static tests were initially performed, followed by single-wheel drops and then two-wheel drops. Six-wheel flat touchdowns were carried out next, followed by sloped touchdowns and, finally, rock-field simulations. Model correlation, performed after testing was complete, followed the same progression. This paper details this test program and the related analytical simulations, with a primary focus on comparing the analysis model with the test data

II. Touchdown Test Facility

The test program was conducted on the JPL campus at a temporary landing test facility created within the JPL Static Test Tower[5]. Two interesting features of the facility are the sand containment structure and the 20 HP electric winch and control system. To maximize economy and flexibility, a sand containment structure was designed to hold up to 40 cubic yards of sand with any surface slope up to 20 degrees**.** See Fig. 2**.** Massive interlocking concrete blocks typically used for earth retention structures formed the sides, while the backwall was constructed from standard steel sheet piling sections cut to 8-foot lengths and bolted to the static test tower. A planar rigid landing surface was created with a 3/8" thick steel plate. This plate was supported from below by a large framework of structural steel angles joined together then backfilled with sand. The steel plate was installed on top of the framework and sand. The resulting steel surface was exceptionally planar, rigid, and smooth.

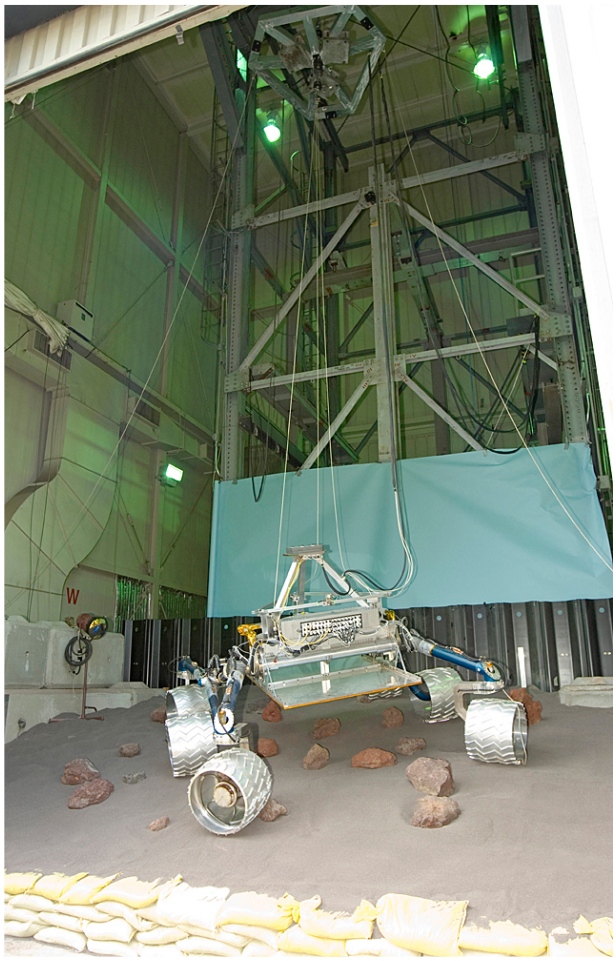


Figure 2. Photograph of the test set-up with a 15° sand landing surface and small rock field.

A 20 HP Thern electric winch with an ABB closed-loop digital controller was used to lower the rover at precisely controlled and adjustable velocities. The precision of this system for delivering the rover at the target velocity was within 5 cm/s, and the repeatability was within 1 cm/s. A second control loop using a National Instruments PXI chassis provided additional capability, including a comprehensive safety interlock system, a very robust means of specifying point-by-point trajectories for raising and lowering the rover, and additional instrumentation and data acquisition. An interesting part of the facility instrumentation is a system for measuring the three-dimensional position of the descent stage by triangulating measurements. The measurements are taken from four separate 1000" string pots which pass through a number of roundabout pulleys mounted on the tower and terminated on a shackle at the end of the winch rope.

Videography was provided using both high-speed video cameras running at 250 frames/sec and consumer-grade high definition video cameras running at 30 fps. The advantage of the HD cameras, which had just debuted on the market as testing was starting, is that they create mpeg-4 files directly to SmartCards. These files need no additional processing or rendering and can be distributed readily to the team and played on any personal computer.

III. Vehicle Design

The test rover is a full-size prototype vehicle built to a 3/8th mass scale with a total mass of 289 kg. The mobility system was built to the MSL flight design that existed at the time of the system Preliminary Design Review (PDR), with a total mass of 161 kg. The mobility system was not mass-scaled, due to the challenges of scaling such a complicated design. To ensure the vehicle as a whole met the 3/8th mass target, the remaining mass had to be distributed between three systems as shown in Table 1. The balance mass ensured the test rover had approximately the same CG location as the flight rover design. Vehicle total mass and CG were measured using a special three-point support system.

Table 1. Vehicle Mass Distribution.

Mobility	161 kg
Chassis Structure	55 kg
Balance mass	62 kg
Data Acquisition H/W	11 kg
Total	289 kg

The principal parts of the SCARECROW rocker-bogie mobility system are shown in Fig. 3. Information about the rocker-bogie architecture can be found in Bickler[6]. Rotation of the bogies with respect to the rear rocker takes place about the bogie pivots. Articulation of the rockers takes place by rotation at the main differential pivots. The differential system connects port and starboard rockers and, through a rotational pivot at the center of the top deck, ensures equal yet opposite rotational displacements around the pivots. Through the scissoring action of the rockers, and the independent rotation of the two bogies, this system has excellent capability to conform to irregular surface terrain. A constant-force spring system provides a restoring moment at the bogie pivot to maintain the rear wheels and mid wheels approximately level when hanging under the bridle.

The chassis is a riveted and bonded plate structure made of aluminum with lead ballast mass. Final machining for the three mobility interfaces was done on the assembled chassis after the riv-bonding process was complete.

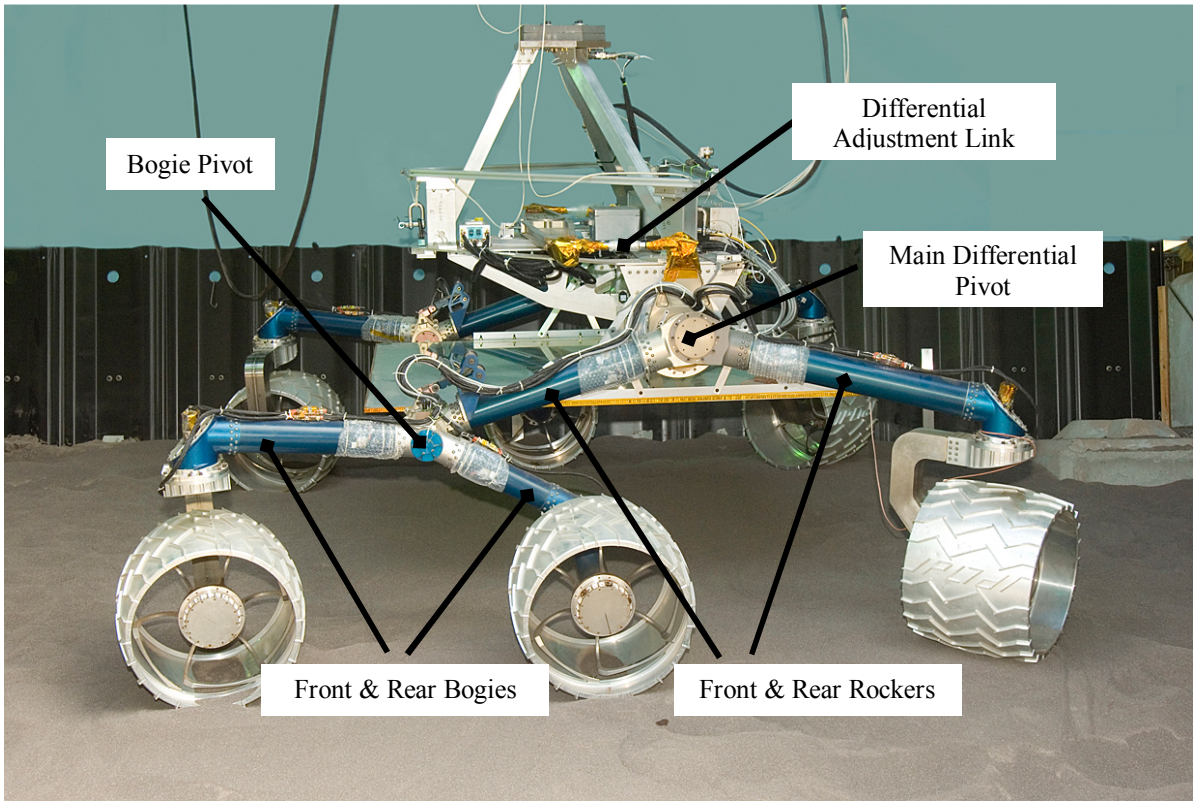


Figure 3. Vehicle pictured in its nominal touchdown posture, with wheels steered 10° rear and 45° front. Vehicle measures 2.75 m front-to-back and 1.1 m tall at the top deck.

IV. Instrumentation

A strain gage system acquired loads in the mobility system on over 50 channels. Each of the eight suspension tubes was gaged with a set of four rectangular rosettes spaced 90 degrees apart and located near the end fitting. To achieve economy in parasitic mass and stiffness due to cabling, only six of the twelve gages on each tube were wired. By reading four axial gages and two 45-degree gages, it was possible to measure axial load, biaxial bending moment, and torque in each tube. In addition to wiring only selected gages, a remarkable 40% reduction in wire count was achieved by using the Anderson loop technique[7] rather than the standard Wheatstone bridge. Locations were precisely marked and gages installed on the bare tubes before they were assembled to their end fittings. Calibration of the force-measuring system was performed on the rover using a series of static loads in well-controlled locations and orientations.

Signals for rover-mounted sensors were acquired with an on-board data acquisition system built around a commercial UEI Data Cube plus auxiliary signal conditioning boards. All data was sampled at 1000 samples/s.

Accelerations during the touchdown event were measured using an arrangement of four triaxial accelerometers mounted to the chassis underside. Rotational potentiometers at the mobility pivot locations, single-axis load cells at the three bridle attach points, and biaxial tilt sensors (DC only) were also located on the rover.

A second set of four triaxial accelerometers was mounted underneath the chassis in a mirror image to the previous set to measure the low frequency and low-amplitude swinging motions of the rover during the descent-to-touchdown phase. Rotational rates on the order of 3 deg/s were expected. These accelerometer measurements were to be converted to rotational accelerations, then integrated to rotational velocities, and ultimately used to compute the attitude and horizontal velocity of the rover[8]. The goal was to measure the complete set of initial conditions at the instant of touchdown. The computational algorithms for postprocessing were written and successfully validated using numerical simulations which approximated the test set-up. In practice, insurmountable difficulties with small accelerometer drift errors due to random noise (see Fig. 4) required the addition of rotational rate gyroscopes to the system, and the goal of precisely measuring all initial conditions at touchdown, except vertical velocity, had to be abandoned. Loss of this capability was a significant loss for the model correlation process.

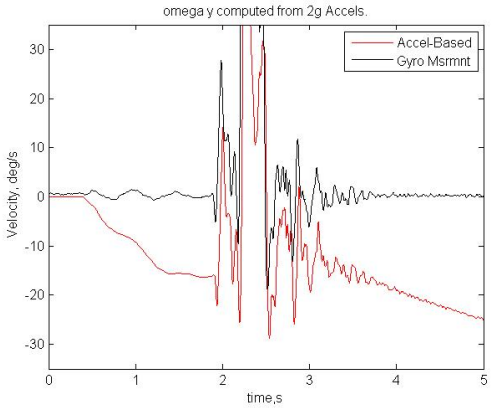


Figure 4. Despite accurate computations of rotational accelerations, even short-term numerical integration of the rotational accelerations resulted in low frequency drifts as seen here (red line).

V. ADAMS Computational Model

An ADAMS computer model of the flight rover was modified to represent the SCARECROW vehicle. In this way, the SCARECROW modeling assumptions are as close as possible to the flight model, ensuring that the predictions and updates to the SCARECROW ADAMS model will be relevant to the flight model.

The model features a rigid mass representation of the chassis, as shown in Fig. 5. The chassis mass properties are assigned explicitly, using solid model calculations that were validated experimentally by both chassis-alone and full-vehicle CG measurements. The mobility system is modeled with flexible beam elements, idealized revolute joints, and lumped masses. The wheel elements are modeled as parasolids, with two toroids located on the inner and outer rim of the wheel. Contact is checked and forces are computed only at the torus shapes on the rims. Friction at the contact between the wheels and the landing surface is assigned values that were directly measured by dragging the rover across both smooth concrete and steel surfaces. No attempt is made in this test program to model touchdowns on sand, rocks, or other terrain types. The titanium wheel flexures are modeled as FIELD[9] elements (a 6x6 matrix of stiffness terms located at the hubs) with off-diagonal terms to capture the

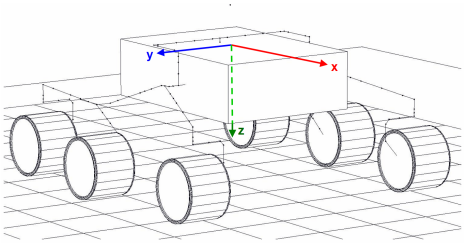


Figure 5. ADAMS model representation of test rover SCARECROW.

coupling inherent in the flexure design. Finite element analysis is used to estimate the wheel flexure stiffness model. Other aspects of the ADAMS flight model have been presented previously[2].

The bridles and winch rope are modeled with linear tension-only SFORCE[9] elements. The descent stage mock-up is represented with a lumped mass having only translational mass.

Finite element modeling of the chassis and mobility system, with wheels pinned to the ground, shows that chassis flexibility starts to couple with mobility system modes at about 20 Hz. This provides a good approximation of the valid frequency range of the ADAMS model.

VI. Static Measurement Results

A suite of static load tests provided both strain gage calibration data and vertical and lateral stiffness measurements. To ensure that load application points and load paths were very well known, the wheels of the vehicle were removed and replaced with aluminum boots. Each boot was mounted at the hub-wheel interface and featured a single roller-caster precisely positioned to eliminate or minimize off-axis moment and torque. The stiffness of the boots was designed so that they contributed less than 10% to the vertical deflections as estimated by pre-test models. Test measurements confirmed the pre-test predicted deflections.

Figure 6 depicts the test set-up for bending moment measurements on the rear rocker. An example of the quality of the strain gage calibration data resulting from this test is shown in Fig. 7. Two moments per side, as computed from measured strain signals, are plotted against the applied load measured with precision scales underneath the special boots (solid-color lines in Fig. 7). The black squares show the analytical predictions based on load and lever-arm distance to the gages, and the solid black lines represent an error band of ±5% of the moment values. These lines aid in assessing the off-axis moments, represented by those lines seen to be well within the error bands. In all, nine separate test configurations in the lateral and vertical directions were used to gather load-deflection and strain gage calibration data.

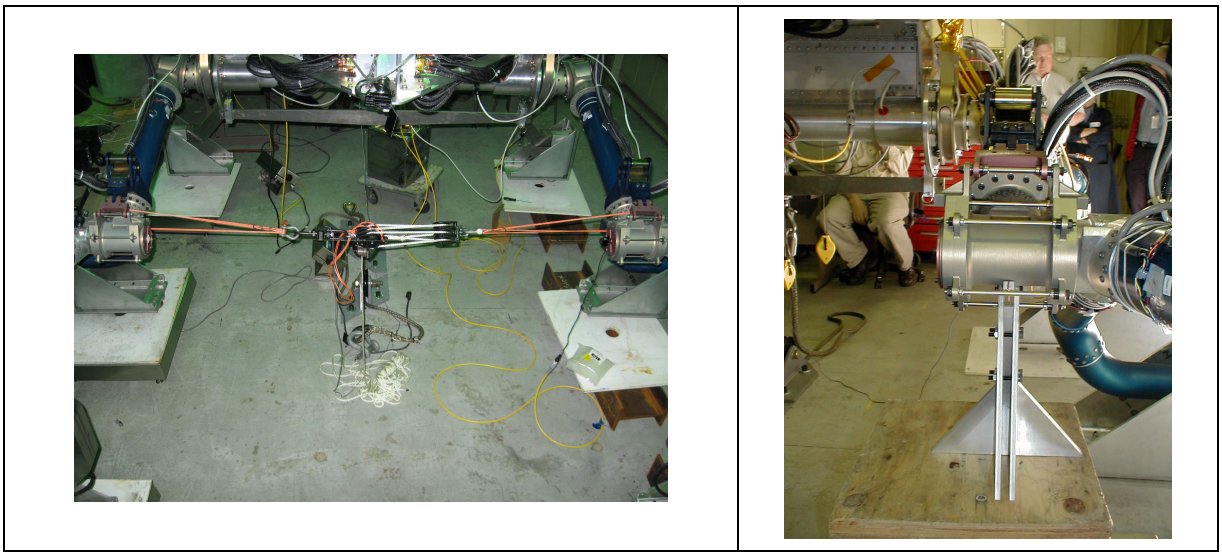


Figure 6. The rover with its wheels off undergoing lateral (left photo) and vertical (right photo) load-deflection testing. Note how the bogie pivots were supported by stands to precisely control the load path.

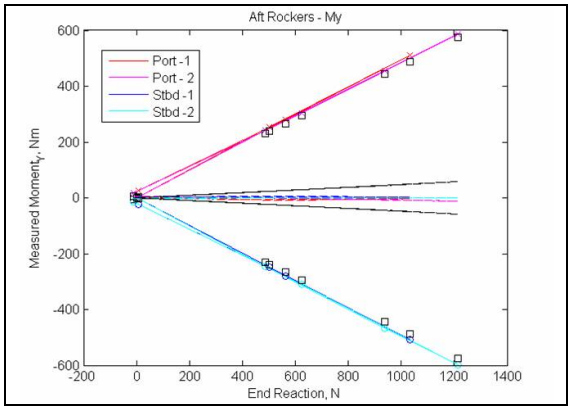


Figure 7. Rear rocker moments computed from strain measurements and load/lever-arm measurements showing excellent agreement.

An additional example of measured data is shown in Fig. 8, where the nonlinear moment-rotation behavior of the rocker-differential pivot and the chassis interface has been measured. By simultaneously measuring the translational displacements of the front and rear rockers, it has been possible to determine the bending stiffness of the front rockers, the nonlinear moment-rotation, and the dead-zone of the pivot mechanisms and chassis flexibility. A companion graph provides stiffness data for the aft rocker and also corroborates the information, through the Maxwell-Betti Reciprocal Theorem.

One outcome of the strain gage calibration tests is that it was not possible to calibrate the axial gages directly. Due to the shallow angle of the suspension tubes, only a small component of the reaction load is projected as axial load in the tube. Consequently, nearly 99% of the strain at the gages was associated with internal moment and only 1% with axial load. The practical consequence of not directly calibrating the axial gages is small, because the same gages were calibrated with a moment loading with excellent results.

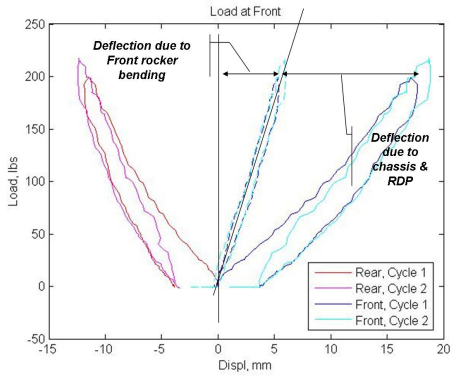


Figure 8. Translational load-deflection measurements in which lateral load is applied to front rockers and displacement is measured at both front and rear rockers.

Model updating to incorporate the test data was largely heuristic, with a focus on areas that had a coincidence of compliance and known or suspected model parameter uncertainty. Comparisons between static stiffness measurements and the ADAMS computer model are shown in Table 2 and Fig. 9. The load-deflection curves in Fig. 9 clearly illustrate the nonlinear stiffening nature of the vehicle. It is immediately apparent that the Generation 1 ADAMS model agrees well at higher load but does not capture the softer stiffness at low loads. This is attributed to the lack of modeling detail. The dynamic relaxation process[10] was used to generate static deflection estimates.

Table 2. Summary of test-analysis stiffness agreement before and after model updating.

Load and Msrmt Direction	Load Location	Measurement Location	Stiffness (N/mm)		Error Range	Adams Predictions…
			Experimental	Adams		
1st Generation Model						
Lateral	Front Rocker	Front Rocker	160	200	20 to 30%	**STIFF**
	Rear Rocker	Rear Rocker	230	220	+/-5%	---
Vertical	Chassis Between MDP Pivots	MDP	1100	1000	0 to 10%	**COMPLIANT**
		Bogie Pivot	1900	1800	0 to 10%	**COMPLIANT**
		Chassis Tail	980	920	0 to 10%	**COMPLIANT**
2nd Generation Model						
Lateral	Front Rocker	Front Rocker	160	160	+/-5%	---
	Rear Rocker	Rear Rocker	230	220	+/-5%	---
Vertical	Chassis Between MDP Pivots	MDP	1100	1000	0 to 10%	**COMPLIANT**
		Bogie Pivot	1900	1900	+/-5%	---
		Chassis Tail	980	1000	0 to 10%	**STIFF**

VII. Wheel Drop Results

A series of 37 simple wheel drop tests was conducted in which either one or both front wheels was suddenly released from a supported condition to fall a distance of approximately 13 cm onto the concrete floor. The rover was not supported by bridles for these tests. Owing to the relatively simple boundary conditions, these tests provided the simplest look at model performance. Because the wheel drop is essentially an impact event of relatively short duration, it was useful to examine not only the time but also the frequency domains.

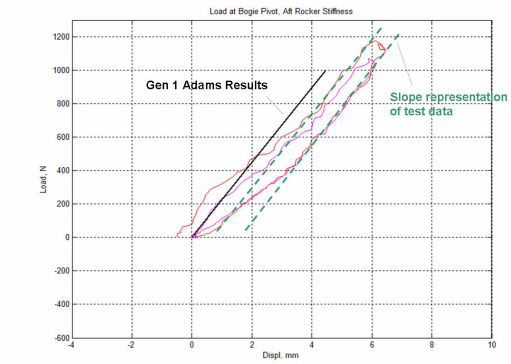


Figure 9. Lateral rear rocker load-deflection measurements showing excellent test-analysis agreement. Dashed lines are tangent stiffness estimates used for quantitative comparisons.

An example of the test-analysis comparison is shown in Fig. 10. All test and analysis data in this series has been low-pass filtered. Data in Fig. 10 is representative of the very good test-analysis agreement for vertical quantities,

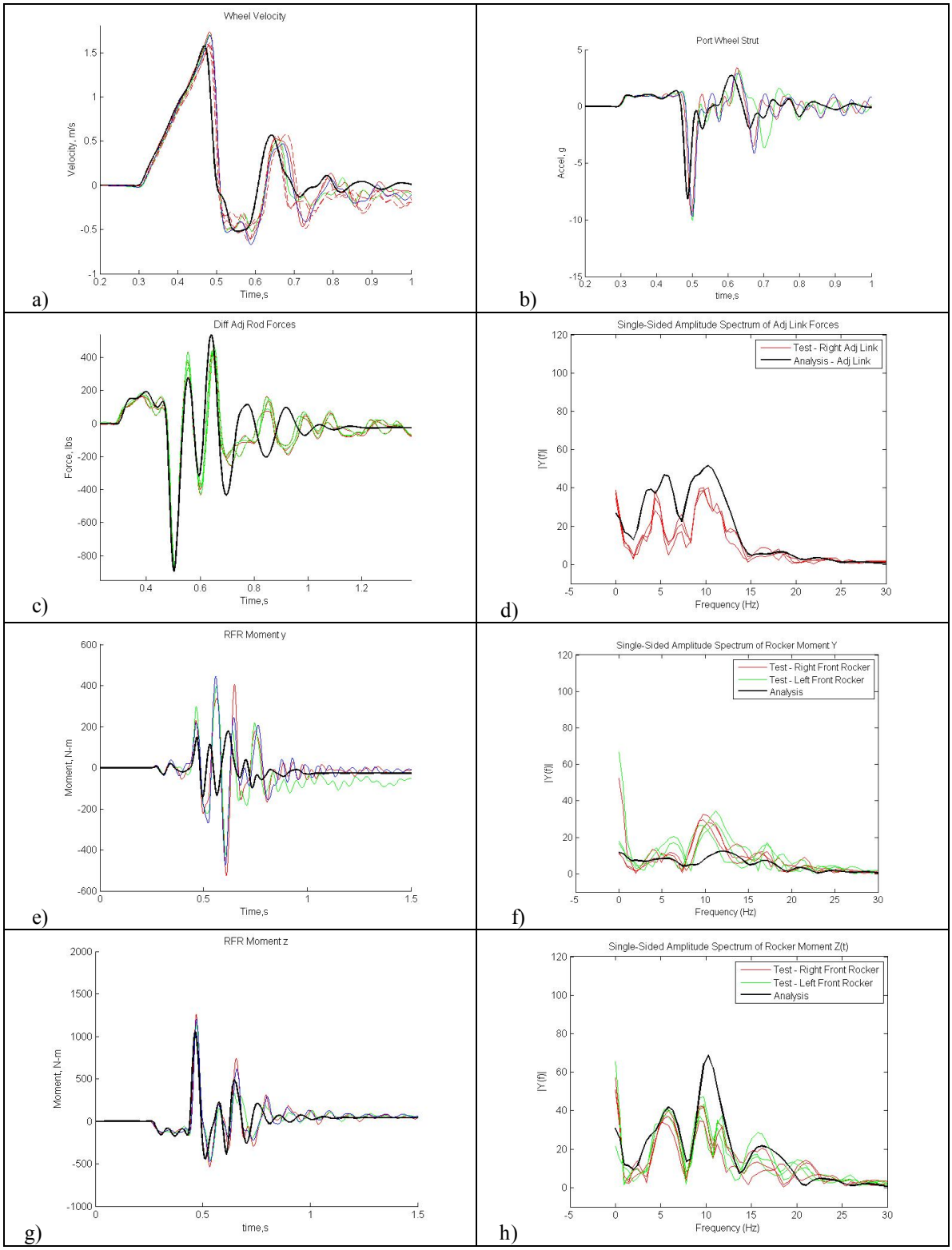


Figure 10. Three nominally identical drops of both front wheels simultaneously, compared to analysis predictions (black lines) show the repeatability typically found in the wheel-drop test series.

but some differences exist for lateral quantities, including front rocker torsion.

As part of the updating process, the rigid chassis was replaced with a flexible-modes representation using ADAMS/Flex. It was found that the flexible model of the chassis resulted in better agreement of some of the force quantities, most notably the differential adjustment link forces. A suitable approximation to the unmodeled chassis compliance was achieved by reducing the bending stiffness of the differential horizontal swing arm in the rigid chassis model.

The frequency domain data suggests that response in the 10-12 Hz range is not being well predicted. Studies conducted during this correlation activity suggest that enhancements may be possible in the modeling of the wheel stiffness matrix, and possibly in the assumed geometric model for wheel-ground contact. The flexibility of the chassis, especially at the central differential pivot, also plays a role in test-analysis agreement.

VIII. Touchdown Results

More than 80 touchdown tests were performed during the program, as cataloged in Table 3. Touchdown velocities ranged from 0.4 m/s up through 1.4 m/s. For sloped-surface touchdowns, 36 of the 52 tests were conducted with the rover heading south (front wheels pointing directly down the slope). The remainder was mostly with the rover heading east (transverse to the slope). These directions were chosen either because they would give the highest loads, because there was a better chance of repeatability than there would be for tests with an oblique heading, or because there was no clear preference for any other heading.

Table 3. Touchdown Terrain Summary.

	# of Tests	Vel. (m/s)
Level Concrete Floor	7	0.4, 0.8, 1.0
Level Floor with single 25cm rock	4	1.0
Level Floor with single 60cm rock	3	1.0
Level Sand @ 0.5m depth	15	0.8, 1.0, 1.2, 1.4
15° Sand	7	0.5, 1.0
15° Sand + Small Rocks	2	0.8, 1.0
15° Rigid Plate	18	0.5, 0.8. 1.0
15° Rigid Plate + Rocks	25	1.4

A subset of the touchdown tests was dedicated to gathering data for model correlation. Examples of some of these data are provided in Fig. 11, where measurements from four sequential touchdown tests at 1 m/s on the level concrete floor are shown. This data has been postprocessed with a low pass filter. The repeatability of the data appears to be very good, but critical examination shows variability in peak

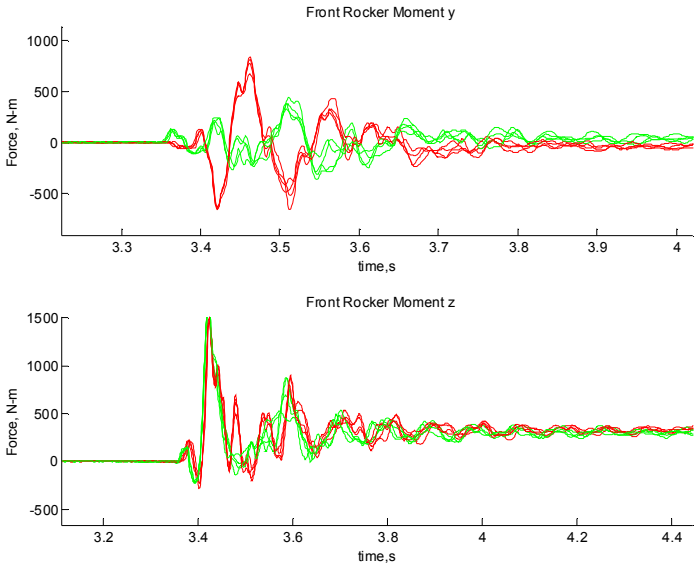


Figure 11. Front Rocker Moment time histories for four touchdowns on level ground. Starboard side (green) and port side (red).

quantities. It is also evident that the Moment y response is not symmetric between the port and starboard sides (red

and green lines, respectively). The reason for this is not understood. It is also important to note that the bogie system has a natural angular bias of 3° to 4°, such that the rear wheels hang lower than the mid wheels, as seen in Fig. 12.

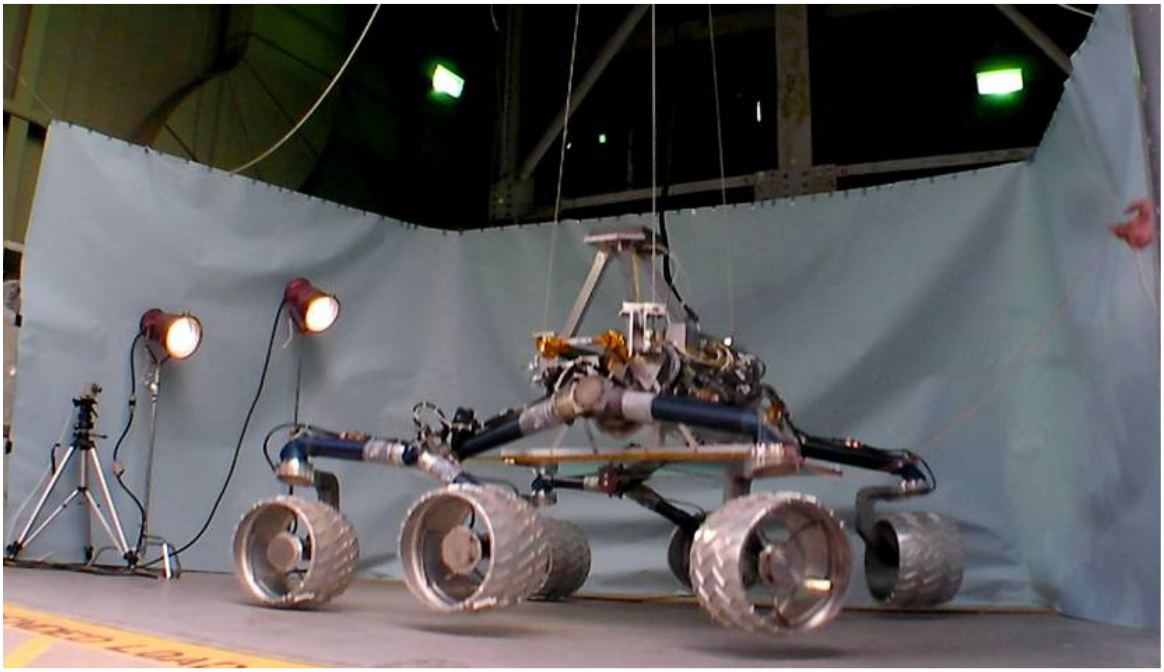


Figure 12. A single video frame provides valuable information at the instant of touchdown.

The variability associated with the peak force measurements is summarized in Table 4. The majority of the spread in the measurements is attributed to small variations in initial conditions other than touchdown speed, as speed itself has been determined to have low variability.

Table 4. Summary of peak load statistics measured for various landing configurations.

Test Series	# of tests	T/D Vel. (m/s)	Accel -x (g)	Accel -y (g)	Accel -z (g)	Link Forces (N)	Port Fwd Rocker Moment (N-m)	Stbd Fwd Rocker Torque (N-m)	Port Fwd Bogie Moment (N-m)	Port Fwd Bogie Torque (N-m)
Flat - Rigid	4	1.0								
Mean			2.4	2.0	4.5	3529	1603	238	632	454
Coeff. Of Variation			13%	16%	3%	4%	1%	19%	13%	10%
Flat - Sand	4	1.0								
Mean			1.2	1.6	2.9	3302	1144	321	451	194
Coeff. Of Variation			22%	11%	15%	6%	17%	16%	9%	18%
15°- Rigid	4	1.0								
Mean			2.5	1.9	4.7	6675	1479	395	595	367
Coeff. Of Variation			12%	10%	17%	2%	5%	29%	11%	12%
15°- Sand	2	1.0								
Mean			1.3	1.2	2.4	5429	945	210	318	190
Coeff. Of Variation			6%	10%	7%	2%	9%	19%	2%	8%

Test measurements were low-pass filtered before comparison to the ADAMS predictions. Agreement between test and analysis for the final updated model is seen in Fig. 13 and Fig. 14. Qualitative agreement of analysis to test is seen to be very good. It is evident that the instant of peak loading does not correspond to the first instant of contact with the surface. Typically, the rover makes contact and the mobility system articulates as it conforms to the surface. Large rotational displacements of the linkages and rigid body motions of the chassis can occur in this phase. The peak loads typically occur when the articulation stops and the load path stiffens. It follows that accurate prediction of response time histories will depend on accurate simulation of a number of events, and that the longer into the event that the peak load occurs, the more difficult it becomes to predict accurately. Order of wheel contact, contact rebound velocities, friction and sliding during contact, mobility system articulation, and bridle interaction are all aspects that need to be captured accurately for accurate time histories. Note in particular that some of the bridle loads persist well into the touchdown event, yet others rapidly diminish. Bridle unloading and reloading can occur. The implication is that precise prediction of rover loads will be a function of bridle load, which in turn is a function of descent stage motions. The descent stage, winch rope, and winch motor and controller form a nonlinear dynamic system unto themselves, one that experiences a step-function unloading when the rover touches down. This effect is more important for sloped surfaces than it is for flat surfaces, because on flat surfaces bridle unloading is essentially instantaneous.

Winch rope stiffness and damping were the first parameters adjusted in the model. This is despite having made experimental measurements of stiffness and damping on a length of the same winch rope before it was installed on the winch drum. It is likely that within the frequency range of interest, the coupled winch motor, controller, and rope system would exhibit different dynamics than the rope alone. The behavior of this coupled system was captured by adjusting the parameters of the rope. Test-analysis agreement improved significantly.

The next parameter adjusted was the 3° to 4° bias angle at the bogie pivot. This adjustment brought the time history agreements much closer, especially for touchdown on flat surfaces. It was also necessary to add an accurate time-varying length of winch rope above the descent stage in order to capture the lateral/pendulum motion of the descent stage. It was also found that a nonlinear bridle stiffness model performed better than a linear stiffness model. In a number of landing scenarios, it was noted that the wheels re-steered themselves a noticeable amount during the simulation, but this was not observed in test.

A quantitative summary of the peak values from test and analysis is provided in Table 5 for touchdown velocity of 1.0 m/s. Averaging of the data from both sides of the vehicle has been used in summarizing the south-heading results, but both sides of the vehicle have been reported for east results due to asymmetry in the responses. The majority of the analysis results fall within the range measured in the test. Notable exceptions include the chassis accelerations, which are mostly overpredicted, and the front rocker torsional load, which is underpredicted. The resultant moment component agrees well because it is frequently dominated by the component associated with vertical load, so any differences in the lateral load component contribute less to the resultant moment. The wheel drop test series uncovered differences in these lateral components.

When drawing conclusions about the quality of model predictions, the variability of test data must be remembered. The test apparatus did not allow the precise control, nor the replication, of initial rover conditions. Reasonable care was made to set up and orient the rover for each test, but it was not possible to measure the complete set of initial conditions at the instant of touchdown. Studies underway suggest that small differences in initial conditions have a large influence on peak loads.

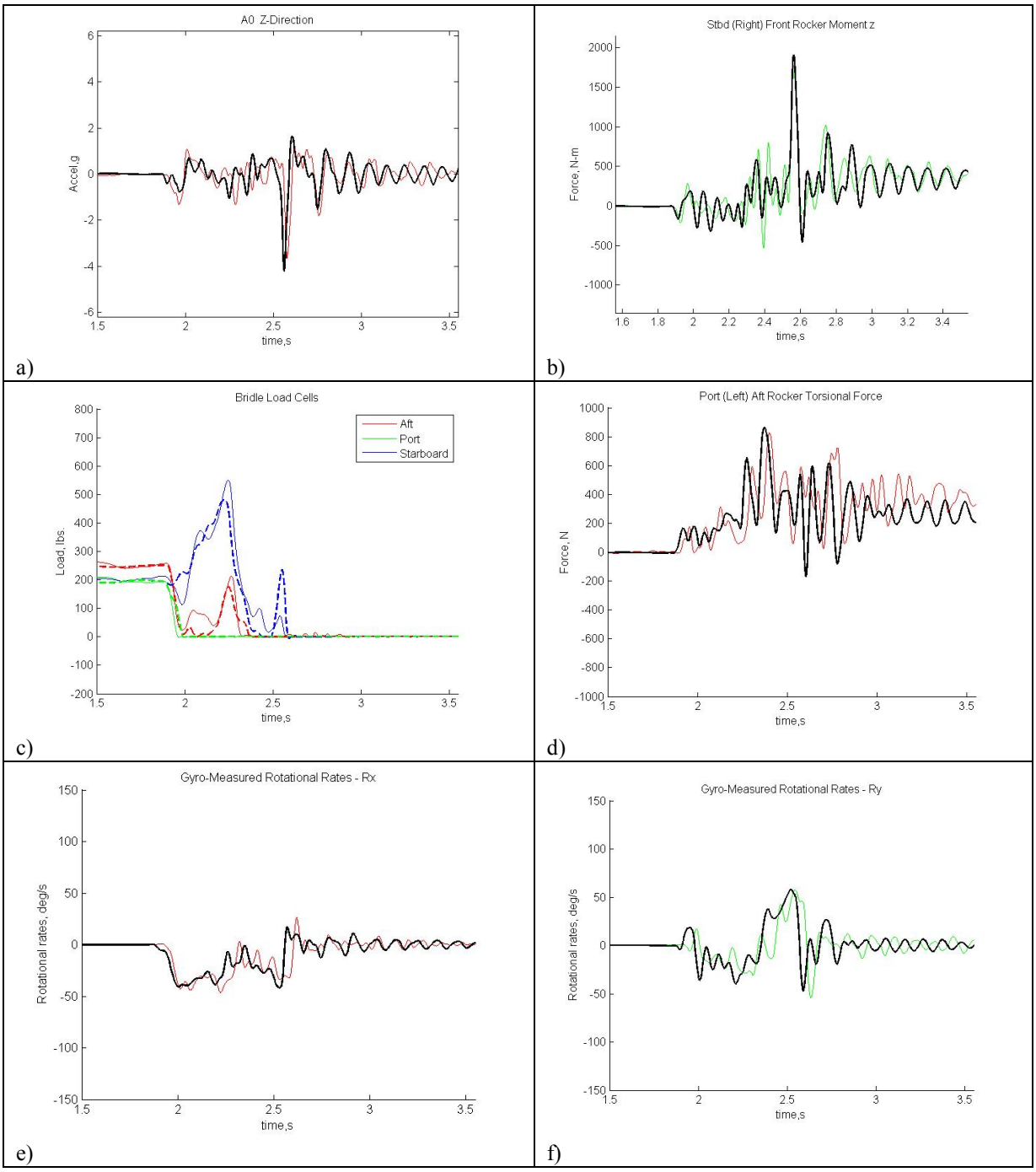


Figure 13. Test-analysis comparison for a single touchdown event, rover heading east, touchdown velocity 1m/s, on a 15° slope showing good qualitative agreement. Black or thick lines represent analysis predictions.

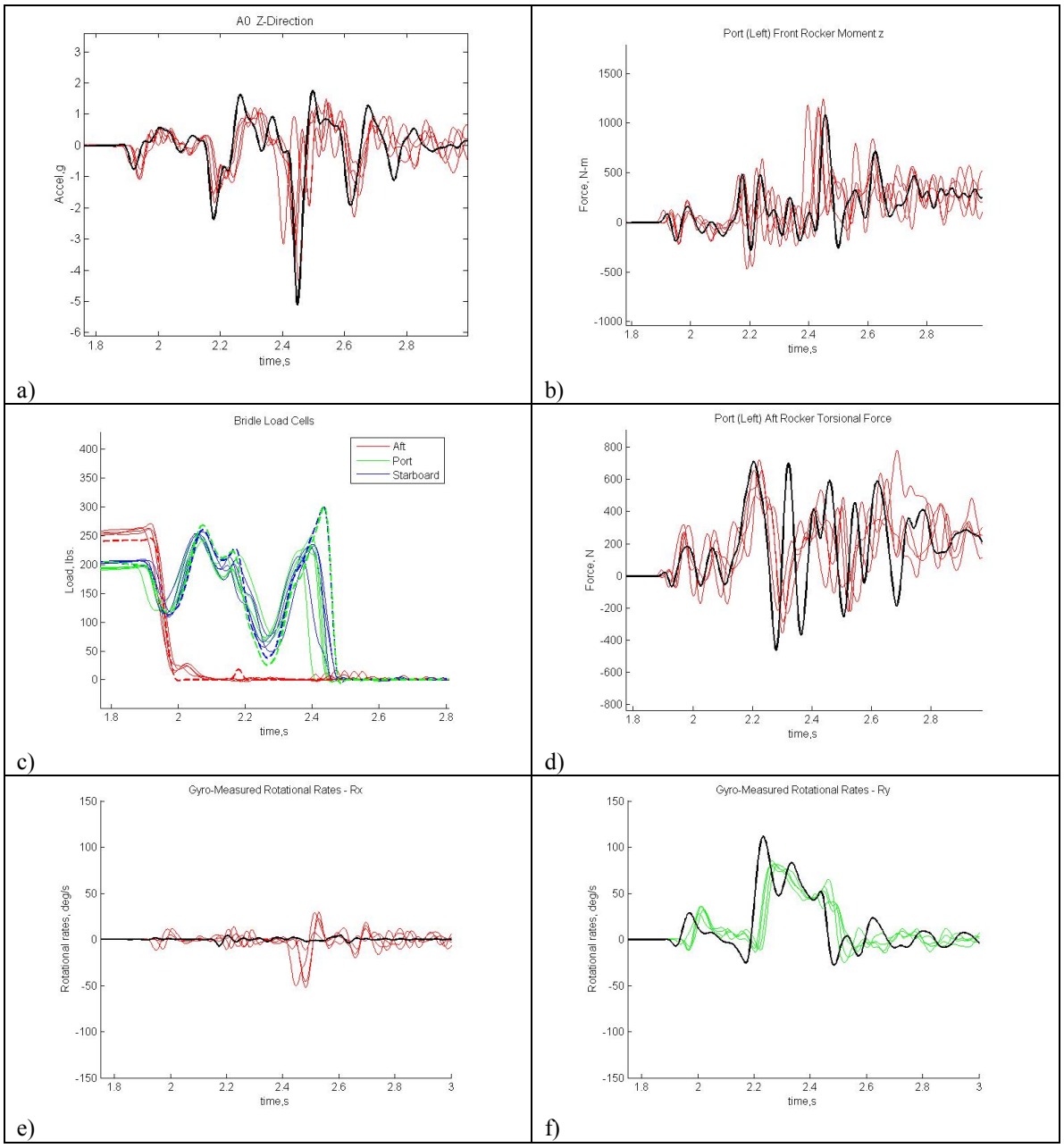


Figure 14. Test-analysis comparison for a series of four sequential touchdown events, rover heading south, touchdown velocity of 1 m/s, on a 15° slope. Black or thick lines represent analysis predictions.

Table 5. Peak response quantities from test and analysis. All data has been filtered with a low pass filter.

SOUTH Heading						
	Accel -x (g)	Accel -y (g)	Accel-z (g)	Link Load (N)	Fwd Rocker Mom. (N-m)	Fwd Rock Torsion (N-m)
Test Max	1.5	1.2	4.5	6559	1385	447
Test Min	1	0.6	3	6364	1250	212
Analysis	1.4	0.3	5.1	7182	1050	122
	Aft Rock Mom. (N-m)	Aft Rock Torsion (N-m)	Fwd Bogie Mom. (N-m)	Fwd Bogie Torsion (N-m)	Aft Bogie Mom. (N-m)	Aft Bogie Torsion (N-m)
Test Max	1506	782	648	329	595	331
Test Min	1441	603	398	241	422	165
Analysis	1420	750	400	305	494	140
EAST Heading						
	Accel -x (g)	Accel -y (g)	Accel-z (g)	Link Load (N)	Fwd Rocker Mom. (N-m)	Fwd Rock Torsion (N-m)
Test Max	1.3	1.7	3.7	3564	1934	699
Test Min					1166	610
Analysis	0.9	2.1	4.1	3128	1992	534
					1143	530
	Aft Rock Mom. (N-m)	Aft Rock Torsion (N-m)	Fwd Bogie Mom. (N-m)	Fwd Bogie Torsion (N-m)	Aft Bogie Mom. (N-m)	Aft Bogie Torsion (N-m)
Test Max	1683	827	635	238	655	362
Test Min	1284	791	525	234	380	388
Analysis	1272	861	474	360	604	593
	1684	622	330	242	452	330

IX. Loads Effects of Sand and Rocks

A partial picture of the peak landing loads difference between rigid planar surfaces and sand surfaces, both flat and sloped, is shown in Table 6. Each row in the table is based on the average measurements of a small number of touchdown tests. For the majority of the data contributing to each row, the variability of peak loads is small, with the notable exception of the Starboard Front Rocker Torque, where the variability was found to be large. It is not understood why these particular data are so variable. The absence of data in some cells is indicative of troubles with the Starboard Rear Rocker strain gage loop circuitry. This data shows how the ratio varies with each measurement location, as well as with touchdown velocity. It also lends credence to the assumption that rigid surface landings bound the event from a loads perspective.

Table 6. Peak loads from rigid landings compared with peak loads from sand landings.

Test Series	T/D Vel (m/s)	Accel-x (g)	Accel-y (g)	Accel-z (g)	Link Force (lbs)		Front Rckr Moment (N-m)		Front Rckr Torque (N-m)		Rear Rckr Moment (N-m)		Rear Rckr Torque (N-m)	
					PORT	STBD	PORT	STBD	PORT	STBD	PORT	STBD	PORT	STBD
Flat Rigid	0.8	1.82	2.40	4.18	849	839	1292	1494	408	285	1251	-	633	-
Flat Sand	0.8	0.73	0.84	1.61	582	598	513	802	187	187	781	999	395	442
Ratio (sand / rigid)		**0.4**	**0.3**	**0.4**	**0.7**	**0.7**	**0.4**	**0.5**	**0.5**	**0.7**	**0.6**	**-**	**0.6**	**-**
Flat Rigid	1	2.38	1.98	4.54	798	789	1603	1720	507	238	1585	-	1042	-
Flat Sand	1	1.16	1.63	2.86	737	746	1144	1159	443	321	1307	1369	455	700
Ratio (sand / rigid)		**0.5**	**0.8**	**0.6**	**0.9**	**0.9**	**0.7**	**0.7**	**0.9**	**1.3**	**0.8**	**-**	**0.4**	**-**
15°Rigid	1	2.48	1.94	4.73	1498	1500	1479	1608	480	395	1681	-	743	-
15°Sand	1	1.26	1.23	2.44	1227	1208	945	1108	442	210	1282	-	495	-
Ratio (sand / rigid)		**0.5**	**0.6**	**0.5**	**0.8**	**0.8**	**0.6**	**0.7**	**0.9**	**0.5**	**0.8**	**-**	**0.7**	**-**

Another interesting comparison is between measurements of landing on rigid planar slopes with rocks and without rocks, which has been summarized in Table 7. The first two tests, Steel15Rock_01 and _02, are planar

surfaces with a rock placed at the toe of the slope, so that the rover slides into the rock after touchdown. The loads generated by the rover sliding into the rock were smaller than those of the preceding touchdown event, so these two tests effectively represent the planar-no-rock touchdown. Tests _12 through _15 consist of a single 60cm rock underneath the rear starboard wheel, where the wheel hits either the top or uphill face of the rock in _12 and _13, and the top or downhill face of the rock in _14 and _15 (see Fig. 15). Inspection of the peak load data shows that suspension tube loads and chassis accelerations can be considerably higher when landing on rocks. However, the peak adjustment link loads are somewhat lower for these rock landings. Interestingly, some of the most severe loading occurs on the port side. This might be explained by the scissoring action of the differential lifting the port front wheel higher than it would without a rock present, setting up a greater fall distance for the front wheel.

Table 7. Peak forces and accelerations for planar rigid landings (tests _01 and _02) compared to planar rigid with a single 60cm rock (tests _12 through _15).

Test Name	T/D Vel (m/s)	Chassis Accel-x (g)	Cahssis Accel-y (g)	Chassis Accel-z (g)	Link Force (lbs)	
					Stbd	Port
Steel15Rock_01	1.4	2.35	1.73	3.2	1721	1724
Steel15Rock_02	1.4	1.69	1.32	3.3	1308	1302
Steel15Rock_12	1.4	2.08	1.4	5.14	1044	1023
Steel15Rock_13	1.4	1.6	1.75	4.97	1502	1496
Steel15Rock_14	1.4	1.74	1.16	3.33	1144	1121
Steel15Rock_15	1.4	1.74	1.27	3.82	1081	1081

Test Name	T/D Vel (m/s)	Front Rckr Moment (N-m)		Front Rckr Torque (N-m)		Rear Rckr Moment (N-m)		Rear Rckr Torque (N-m)	
		Port	Stbd	Port	Stbd	Port	Stbd	Port	Stbd
Steel15Rock_01	1.4	1754	1726	861	462	1442	-	1175	-
Steel15Rock_02	1.4	1678	1332	585	540	1898	-	768	-
Steel15Rock_12	1.4	2824	1428	504	479	2528	-	1070	-
Steel15Rock_13	1.4	2339	1585	407	965	2289	-	903	-
Steel15Rock_14	1.4	2499	1445	391	856	1640	-	794	-
Steel15Rock_15	1.4	1957	1526	484	530	1987	-	759	-

Test Name	T/D Vel (m/s)	Front Bogie Moment (N-m)		Front Bogie Torque (N-m)		Rear Bogie Moment (N-m)		Rear Bogie Torque (N-m)	
		Port	Stbd	Port	Stbd	Port	Stbd	Port	Stbd
Steel15Rock_01	1.4	658	445	493	324	584	550	352	339
Steel15Rock_02	1.4	555	538	381	519	635	490	484	440
Steel15Rock_12	1.4	781	688	484	412	986	466	323	312
Steel15Rock_13	1.4	639	605	364	359	868	662	413	444
Steel15Rock_14	1.4	591	885	318	437	676	705	371	336
Steel15Rock_15	1.4	459	568	411	286	696	528	463	628

X. Conclusion

A full size, 3/8th mass test program has been conducted to study the Skycrane landing event. A subset of the tests was performed specifically for model validation and updating. An ADAMS model of the test hardware was developed in parallel with the testing.

Correlation of the model with static load test data provided improved mobility stiffness estimates. Static test data also demonstrated the nonlinear stiffening nature of the rover mobility system under vertical load and the nonlinear response due to the angular dead-zone at the main differential pivot under lateral load. Comparison of wheel drop measurements with analysis showed that response sensitivities exist due to the coupling terms of the wheel flexure model and also due to the compliance of the chassis structure.

In the touchdown test model correlation, it was not possible to completely separate test and analysis differences due to lack of knowledge of initial conditions. Response quantities were determined to be sensitive to bogie angular position at the instant of touchdown and to bridle loads as influenced by descent stage motions and bridle load-displacement relationships. Overall, however, in consideration of the entire suite of test data and the associated variablity, very good agreement has been achieved on many relevant response quantities.

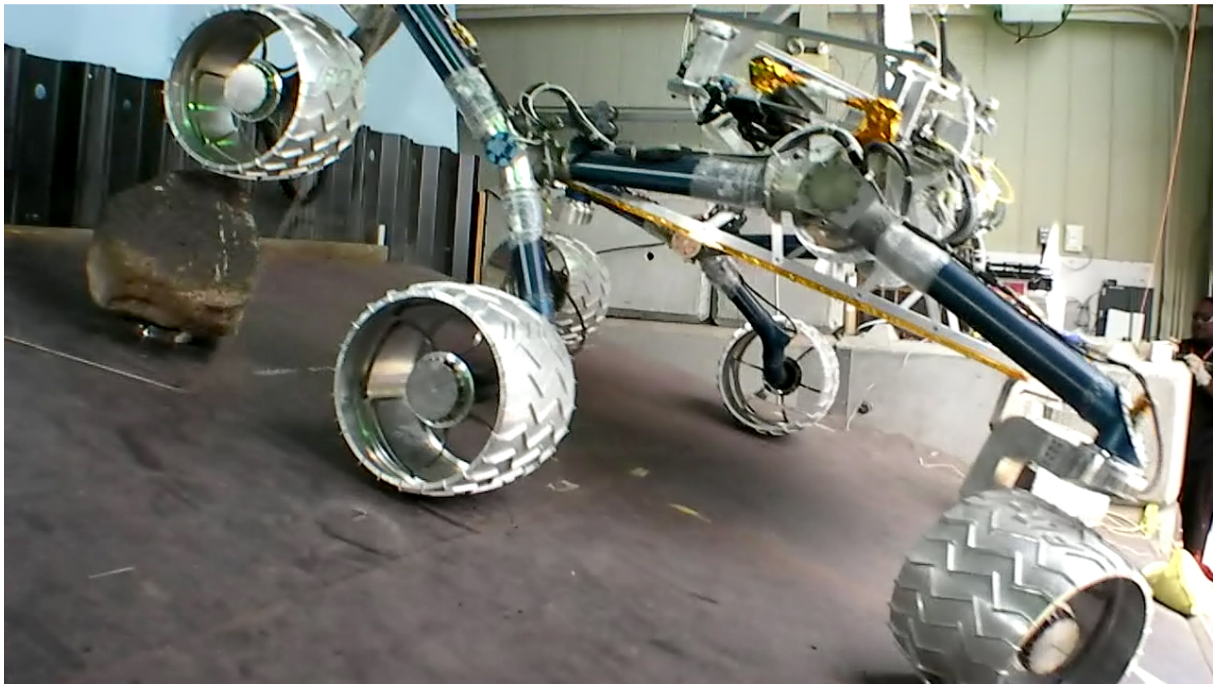


Figure 15. Rover photographed during touchdown on 15° slope with a single 60cm rock.

Acknowledgments

Numerous individuals from the MSL project team have made this work possible, and their contributions are sincerely acknowledged. Tommaso Rivellini, Christopher Voorhees, Jeff Umland, Richard Rainen, Jaime Waydo and Chia-Yen Peng contributed greatly to the success of this program. In particular, Jaime Waydo and the MSL mobility team accomplished the detailed design, fabrication, and assembly of the SCARECROW mobility system while continuing their demanding duties on the flight design. The talented and dedicated test crew, Larry Broms, Charles Morris, Al Edwards, Tuan Ngyuen, Dan Linehan, and Charles Rhodes always got the job done. Many thanks to Collin McEwen of ATA for his contributions during the mass updating phase of computer modeling, and to Mary Baker and Charles Engelhardt of ATA Engineering, who reviewed the manuscript and provided valuable suggestions. This work was performed for the Jet Propulsion Laboratory, California Institute of Technology, sponsored by the National Aeronautics and Space Administration.

References

[1] Steltzner, A., D. Kipp, A. Chen, D. Burkhart, C. Guernsey, G. Mendeck, R. Mitcheltree, R. Powell, T. Rivellini, M. San Martin, D. Way "Mars Science Laboratory entry, descent, and landing system," *IEEE Aerospace Conference*, Mar 4-11 2006, Big Sky, MT.

[2] Peng**,** C-Y., G. Ortiz, T. Rivellini, D. Lee, S-S. Lih, J. Waydo, C. White, S. Haggart, C. Voorhees, R. Rainen, "Dynamic Simulations of Mars Science Laboratory EDL Landing Loads and Stability." *IEEE Aerospace Conference*, 2007, Big Sky, MT.

[3] Laurenson, R.M., Lelliere, R.A., and McGehee, J., "Analysis of Legged Landers for the Survivable Soft Landing of Instrument Payloads," Journal of Spacecraft, Vol. 10, No. 3, 1972.

[4] Adams, D., "Mars Exploration Rover Airbag Landing Loads Testing and Analysis," 45th AIAA/ASME/ASCE/AHS/ASC Structures, Structural Dynamics, and Materials Conference, Palm Springs, CA, April 2004.

[5] White, C.V., Frankovich, J.K., Yates, P., Wells, Jr, G., Losey, R., "A Capable and Temporary Test Facility on a Shoestring Budget: The MSL Touchdown Test Facility." *2008 Aerospace Testing Seminar*, Manhattan Beach, CA, 2008. *Submitted for Publication*

[6] Bickler, D., "Roving Over Mars," *Mechanical Engineering*, April 1998, pp. 74-77.

[7] Anderson, K. "The new current loop: an instrumentation and measurement circuit topology," *IEEE Transactions on Instrumentation and Measurement,* Volume 46, Issue 5, Oct. 1997.

[8] Mital, N.K., King, A.I., "Computation of Rigid-Body Rotation in Three-Dimensional Space from Body-Fixed Linear Acceleration Measurements." *ASME Journal of Applied Mechanics*, Vol. 46, December 1979, pp. 925-930.

[9]ADAMS, Software Package, Ver. 2007, R1, MSC Software, Santa Ana, CA, 2007.

[10] Underwood, P. "Dynamic Relaxation," in Computational Methods in Transient Analysis, Belytschko T, and Hughes, TJR, 1983, pp. 245-265.